NeuroImage 188 (2019) 102–110

Contents lists available at ScienceDirect

NeuroImage

journal homepage: www.elsevier.com/locate/neuroimage

Accuracy and reliability of [^{11}C]PBR28 specific binding estimated without the use of a reference region

Pontus Plavén-Sigray [a,*], Martin Schain [b], Francesca Zanderigo [c,d], Karolinska [^{11}C]PBR28 study group, Eugenii A. Rabiner [e], Roger N. Gunn [e,f], R. Todd Ogden [c,d,g], Simon Cervenka [a]

[a] Centre for Psychiatry Research, Department of Clinical Neuroscience, Karolinska Institutet, & Stockholm Health Care Services, Stockholm County Council, Karolinska University Hospital, SE-171 76 Stockholm, Sweden
[b] Neurobiology Research Unit, Copenhagen University Hospital, Copenhagen, Denmark
[c] Department of Psychiatry, Columbia University, New York, NY, USA
[d] Molecular Imaging and Neuropathology Division, New York State Psychiatric Institute, New York, USA
[e] Invicro LLC, London, UK
[f] Division of Brain Sciences, Imperial College London, London, UK
[g] Department of Biostatistics, Mailman School of Public Health, Columbia University, New York, USA

ARTICLE INFO

Keywords:
Positron emission tomography
SIME
[^{11}C]PBR28
Translocator protein
Non-displaceable binding
Reference region

ABSTRACT

[^{11}C]PBR28 is a positron emission tomography radioligand used to examine the expression of the 18 kDa translocator protein (TSPO). TSPO is located in glial cells and can function as a marker for immune activation. Since TSPO is expressed throughout the brain, no true reference region exists. For this reason, an arterial input function is required for accurate quantification of [^{11}C]PBR28 binding and the most common outcome measure is the total distribution volume (V_T). Notably, V_T reflects both specific binding and non-displaceable binding. Therefore, estimates of specific binding, such as binding potential (e.g. BP_{ND}) and specific distribution volume (V_S) should theoretically be more sensitive to underlying differences in TSPO expression. It is unknown, however, if unbiased and accurate estimates of these outcome measures are obtainable for [^{11}C]PBR28.

The Simultaneous Estimation (SIME) method uses time-activity-curves from multiple brain regions with the aim to obtain a brain-wide estimate of the non-displaceable distribution volume (V_{ND}), which can subsequently be used to improve the estimation of BP_{ND} and V_S. In this study we evaluated the accuracy of SIME-derived V_{ND}, and the reliability of resulting estimates of specific binding for [^{11}C]PBR28, using a combination of simulation experiments and *in vivo* studies in healthy humans.

The simulation experiments, based on data from 54 unique [^{11}C]PBR28 examinations, showed that V_{ND} values estimated using SIME were both precise and accurate. Data from a pharmacological competition challenge ($n = 5$) showed that SIME provided V_{ND} values that were on average 19% lower than those obtained using the Lassen plot, but similar to values obtained using the Likelihood-Estimation of Occupancy technique. Test-retest data ($n = 11$) showed that SIME-derived V_S values exhibited good reliability and precision, while larger variability was observed in SIME-derived BP_{ND} values.

The results support the use of SIME for quantifying specific binding of [^{11}C]PBR28, and suggest that V_S can be used in complement to the conventional outcome measure V_T. Additional studies in patient cohorts are warranted.

1. Introduction

The brain immune system has long been hypothesized to play an important role in the development and progression of neurological and psychiatric conditions (Heneka et al., 2015; van der Doef et al., 2015; Wee Yong, 2010). To date, the most common method for measuring immune activation *in vivo* is to use positron emission tomography (PET) to quantify the expression of the 18 kDa translocator protein (TSPO) in the brain (Crawshaw and Robertson, 2017; Venneti et al., 2006). TSPO is located in glial cells, including microglia and astrocytes, and has been considered a marker for activation of these cell types (Liu et al., 2014; Venneti et al., 2013).

* Corresponding author.
E-mail address: pontus.plaven-sigray@ki.se (P. Plavén-Sigray).

https://doi.org/10.1016/j.neuroimage.2018.11.020
Received 18 June 2018; Received in revised form 6 November 2018; Accepted 16 November 2018
Available online 27 November 2018

Table 1
Demographic, genotype and radioactivity information of included datasets.

Dataset	N	HABs	MABs	Females	Males	Mean Age	SD Age	Mean Injected MBq	SD Injected MBq
KI-Database	54	30	24	22	32	45.2	17	411	58.4
TestRetest	11	5	6	5	6	24.5	3.0	373.4	61.4
XBD173 Blocking	5	5	0	0	5	25.2	7.3	335.6	7.4

[^{11}C]PBR28 is a second-generation TSPO radioligand with improved signal to noise ratio (Fujita et al., 2017; Kobayashi et al., 2017; Kreisl et al., 2010) and reliability (Collste et al., 2016; Park et al., 2015) relative to the first generation TSPO radioligand (R)-[^{11}C]PK11195 (Jučaite et al., 2012; Plavén-Sigray et al., 2018). It is arguably the most widely applied second-generation radioligand for examining TSPO levels in psychiatric and neurological disorders (Bloomfield et al., 2015; Chauveau et al., 2008; Collste et al., 2017; Fregonara et al., 2017; Kreisl et al., 2016; Lagarde et al., 2017). An important goal in the field has been the evaluation of [^{11}C]PBR28 as a diagnostic marker and for monitoring treatment strategies that target the immune system of the brain. For this purpose, it is necessary to develop methods that provide reliable, accurate and precise estimates of outcome measures reflecting [^{11}C]PBR28 specific binding to TSPO. Examples of methods that have been used for estimating [^{11}C]PBR28 binding are the unconstrained two-tissue compartmental model (2TCM), graphical and linear models (Ichise et al., 2002; Logan et al., 1996) as well as a modified version of the 2TCM that takes endothelial TSPO binding in blood vessels into account (Rizzo et al., 2014; Veronese et al., 2017). Simplified methods for estimation of binding and uptake has also been proposed, such as using a pseudo-reference region or standardized uptake value ratios (Lyoo et al., 2015; Matheson et al., 2017; Nair et al., 2016).

Since there is no region devoid of TSPO in the brain, full quantification of [^{11}C]PBR28 binding requires measurements of metabolite-corrected radioligand concentrations in the arterial plasma to be used as an arterial input function (AIF) in a kinetic model. When using an AIF, the most straightforward estimate of binding in the brain is the total distribution volume (V_T), which represents the sum of the radioligand specific (V_S) and non-displaceable (V_{ND}) distribution volumes. As such, V_T can only be considered an indirect index of specific binding to TSPO. In contrast, V_S or the non-displaceable binding potential (BP_{ND}=V_S/V_{ND}) are more direct estimates of specific binding (Innis et al., 2007) and should theoretically possess higher sensitivity to detect longitudinal changes or group differences. However, V_S and BP_{ND} calculated directly from the rate constants (estimated using a kinetic model with an AIF) are often unstable and unreliable (Slifstein and Laruelle, 2001; Varnäs et al., 2013), especially for TSPO radioligands (Collste et al., 2016; Jučaite et al., 2012; Plavén-Sigray et al., 2018), and therefore of limited utility in practice.

The kinetic modelling technique Simultaneous Estimation (SIME) aims to derive a reliable, brain-wide estimate of V_{ND} in absence of a reference region (Ogden et al., 2015) and consequently, more stable estimates of specific binding can be obtained. In brief, the method works by identifying the value for V_{ND} that best describes the observed PET data across all brain regions considered in the analysis. So far, SIME has been evaluated for the serotonin receptor 1A radioligands [^{11}C]WAY-100635 and [^{11}C]CUM101. The results showed that SIME obtained estimates that are close to "gold standard" measures of V_{ND} for these radioligands (Ogden et al., 2015). With regards to [^{11}C]PBR28, SIME was recently applied to quantify [^{11}C]PBR28 BP_{ND} in a cohort of healthy controls and patients with Alzheimer's disease (Schain et al., 2018b). That study concluded that SIME appeared to be useful for quantification of [^{11}C]PBR28, because V_{ND} and BP_{ND} were considered clearly identifiable and fell within ranges that were expected based on theory and previous publications. However, it still remains unclear whether [^{11}C]PBR28 V_S or BP_{ND} derived using SIME are unbiased and reliable, as the method has not yet been evaluated in cases for which the true TSPO binding levels were known.

The aim of this study was to evaluate the accuracy and reliability of SIME for estimating [^{11}C]PBR28 V_{ND} and specific binding. To examine accuracy, we a) performed a simulation experiment, b) compared SIME-V_{ND} to V_{ND} estimates obtained from pharmacological competition challenge, and c) compared SIME-V_{ND}, V_S and BP_{ND} values between high affinity binder (HAB) and mixed affinity binder (MAB) subjects in a large group of healthy controls. To examine reliability, test-retest properties of SIME-derived BP_{ND} and V_S values were assessed using a [^{11}C]PBR28 test-retest data set.

2. Methods

2.1. SIME and measures of specific binding

SIME constrains V_{ND} (i.e., K_1/k_2 in a 2TCM) to be the same across a set of regions of interest (ROIs). A grid of possible V_{ND} values is then evaluated as follows: For each possible V_{ND}, all ROIs are simultaneously fitted using a constrained 2TCM (in which K_1/k_2 is forced to be equal to the V_{ND} under evaluation). The corresponding residual sums of squares across time frames and ROIs are then used to build an objective function for the purposes of determining V_{ND}. The coordinate at which the objective function achieves a minimum is considered the optimal estimate of V_{ND} for that PET measurement. For a more detailed explanation of the SIME algorithm see Ogden et al. (2015).

In this study, the SIME-derived estimates of V_{ND} were subsequently used to calculate outcome measures of [^{11}C]PBR28 specific binding according to

$$V_S = V_T - V_{ND} \quad (1)$$

$$BP_{ND} = \frac{V_T - V_{ND}}{V_{ND}} \quad (2)$$

where V_T was independently derived from an unconstrained 2TCM in a target ROI. The primary target ROI used in this study, unless otherwise specified, is the whole grey matter defined using FreeSurfer (v5.0.0, http://surfer.nmr.mgh.harvard.edu/) segmentation. For all kinetic models used in this article (both SIME and unconstrained 2TCM), the whole-blood fraction (vB) was fitted as a free parameter for each ROI, unless otherwise stated.

2.2. Subjects and data

This study includes three different datasets of healthy subjects that underwent PET examinations with [^{11}C]PBR28 (Table 1). All subjects gave written informed consent prior to their participation. The studies conducted in Sweden were approved by the Karolinska University Hospital Radiation Safety Committee and the Regional Ethics Committee in Stockholm, whilst the study conducted in the UK was approved by the West London Research Ethics Committee and ARSAC (Administration of Radioactive Substances Advisory Committee).

Subject eligibility was confirmed via a health screening, evaluation of their medical history, physical and neurological examinations and routine blood tests.

2.2.1. KI [^{11}C]PBR28 database

The Karolinska Institutet (KI) [^{11}C]PBR28 database currently consists of 54 subjects (30 HABs and 24 MABs; 32 males and 22 females) who

participated as healthy controls in a set of previously published (Collste et al., 2016; Tamm et al., 2017; Kanegawa et al., 2016) or ongoing [^{11}C]PBR28 studies. All subjects were examined on the same PET system using identical protocols for radioligand synthesis, acquisition of transmission and emission data (although the duration of the emission scans differed, see below), and image reconstruction and analysis, as described below.

PET measurements were carried out at the PET center at KI, Stockholm, on a High-Resolution Research Tomograph (Siemens Molecular Imaging, Knoxville, TN). Individualized plaster helmets were made for each subject and used with a head-fixation device to minimize head movement during the examinations. A 6-min long transmission scan using a single ^{137}Cs source was carried out prior to each emission scan for attenuation correction. Radiosynthesis of [^{11}C]PBR28 was performed as previously described (Briard et al., 2007). The radioligand was administered as a rapid bolus injected into the antecubital vein. Emission data were acquired for 75 min (N = 19) or 90 min (N = 35) and binned into time frames of length 8 × 10s, 5 × 20s, 4 × 30s, 4 × 60s, 4 × 120s, and 7 × 360s (N = 19) or 9 × 360s (N = 35). PET images were then reconstructed using ordered subsets expectation maximization, including modelling of the point spread function.

For all subjects, arterial blood samples were acquired during the first 5 min of the PET examination using an automated blood sampling system (ABSS, Alogg technologies, Mariefred, Sweden). In addition, manual samples (1–3 mL) were drawn between 1 and 20 min post injection, in 2-min intervals. Afterwards, manual samples were acquired in 10-min intervals until the end of the examination. Radioactivity was immediately measured in a well counter that was cross-calibrated with the PET system. Corresponding plasma samples were obtained by centrifuging the blood samples and measuring radioactivity in the ensuing plasma using the same well counter.

Whole-blood time activity curves (TACs) were obtained by combining the ABSS and manual blood samples curves. The plasma radioactivity curve was generated by multiplying the whole-blood TAC with plasma-to-blood ratios estimated from manual plasma samples. Parent fraction of the radioligand was measured as described previously (Collste et al., 2016). To estimate the parent fraction at intermediate time points, a Hill function was fitted to the measurements and multiplied with the plasma curve to produce the final metabolite-corrected plasma curve used as AIF for each examination.

T1-weighted Magnetic Resonance Imaging (MRI) images were obtained for all subjects on a 3-T General Electric Discovery MR750 system (GE, Milwaukee, WI). ROI delineation was performed using the FreeSurfer software resulting in 12 ROIs: whole grey matter (GM), frontal cortex, temporal cortex, parietal cortex, occipital cortex, limbic lobe, thalamus, striatum, insula, anterior cingulate cortex, posterior cingulate cortex and cerebellum cortex. All ROIs were co-registered to the corresponding PET image, allowing for extraction of regional TACs. Since a subset of subjects in the database underwent only 75 min of PET examination, all TACs in this study were truncated at 75 min to allow for consistent pooling and comparisons, unless otherwise specified.

2.2.2. Pharmacological competition data

Data from five healthy control subjects (all HABs, all males) who participated in a previous pharmacological competition study (Owen et al., 2014) carried out at Invicro LLC London, were reanalysed to examine the correspondence between SIME-V_{ND} and V_{ND} estimates obtained from a XBD173 blocking challenge. After a baseline PET, subjects received an oral dose of the selective TSPO agonist XBD173 (10–90 mg), followed two hours later by a repeat [^{11}C]PBR28 examination. Radiochemistry, imaging protocols, reconstruction, retrieval of TACs and AIF are described in the original study (Owen et al., 2014). For the present reanalysis, 9 ROI TACs were obtained from both the baseline and blocking measurement: frontal cortex, occipital cortex, temporal cortex, parietal cortex, hippocampus, amygdala, thalamus, striatum and cerebellum.

2.2.3. Test-retest data

A subset of subjects (N = 12) in the KI [^{11}C]PBR28 database participated in a test-retest study of [^{11}C]PBR28 (Collste et al., 2016). For six of them, two PET measurements were carried out on the same day, and for the other six, the PET scans were taken 2–5 days apart. One PET examination performed on a HAB subject was shortened (60 min) due to technical reasons, and this participant was therefore excluded from the test-retest analysis in this study. Image analysis and kinetic modelling for all remaining 11 test-retest subjects were carried out as described in section 2.2.1 above.

2.3. Simulations

A simulation experiment was performed with the goal of examining whether SIME-derived V_{ND} values were accurate (low percentage bias) and precise (low CoV) for [^{11}C]PBR28. In brief, noise-free [^{11}C]PBR28 model curves were extracted from a HAB and a MAB subject, from the KI [^{11}C]PBR28 database. We then sampled residuals from fitted ROI TACs (the ROIs are listed above in section "2.2.1. KI [^{11}C]PBR28 database") and added these to the noise-free models curves to create simulated [^{11}C]PBR28 TACs. This procedure was repeated 1000 times for both the HAB and the MAB subject. SIME was applied to each simulated noise-instance and estimates of V_{ND} were obtained and compared against the "true" V_{ND} (from the noise-free model curves) for the underlying subject. In addition to the assessing of accuracy and precision, we also assessed the robustness of SIME. This was done by increasing the noise by 50% in the simulated data by multiplying the sampled residual by 1.5. In each simulation, SIME was performed using a grid of candidate V_{ND} values spanning from 0 to 5 with a step size of 0.01. For an in-depth explanation of the simulation procedure see Appendix A: Supplementary Information.

2.4. XBD173 competition challenge

V_T values for each ROI (listed above in section "2.2.2. Pharmacological competition data") and for each subject were obtained using the unconstrained 2TCM for all baseline and blocking examinations. The revised Lassen plot (Cunningham et al., 2010) was applied to estimate V_{ND} for each subject separately. In addition to the Lassen plot, it has also been suggested that occupancy and V_{ND} can be estimated from a blocking data using multi-level modelling with likelihood-based techniques (Naganawa et al., 2017; Schain et al., 2018a). Here, we employed the Likelihood Estimation of Occupancy (LEO) (Schain et al., 2018a) method to compliment the Lassen plot. LEO has shown to produce accurate estimates of V_{ND} for another radioligand, but a pre-requisite of the model is that the ROI variance-covariance matrix is known. This matrix can be estimated from an independent test-retest dataset from the same radioligand. Hence, we applied LEO to the blocking data to estimate V_{ND}, using the test-retest [^{11}C]PBR28 examinations described above in section 2.2.3. Finally, SIME was applied to all baseline measurements, using a grid of candidate V_{ND} values spanning from 0 to 5 with a step size of 0.005. SIME-derived V_{ND} values were then compared to the outcomes from the Lassen plots and LEO to assess the accuracy (percentage bias) of the SIME method. Both 70 and 90 min TACs were used for SIME, Lassen plot and LEO, in order to examine the stability of V_{ND} over time.

2.5. Differences between HABs and MABs

One aim of the study was to examine differences in SIME-V_{ND}, and ensuing estimates of specific binding, between HAB and MAB subjects. For this goal, SIME (grid spanning from 0 to 5 with a step size of 0.005) was applied to all subjects' ROI TACs in the KI [^{11}C]PBR28 database (see 2.2.1. above). Mean differences in SIME-derived V_{ND} values were then examined between the 32 HAB and 23 MAB subjects. V_T values from GM ROI were also derived for all subjects using the unconstrained 2TCM. GM V_S and BP_{ND} values were calculated using equations 1 and 2. The separation between HABs and MABs using V_T and SIME-derived outcomes

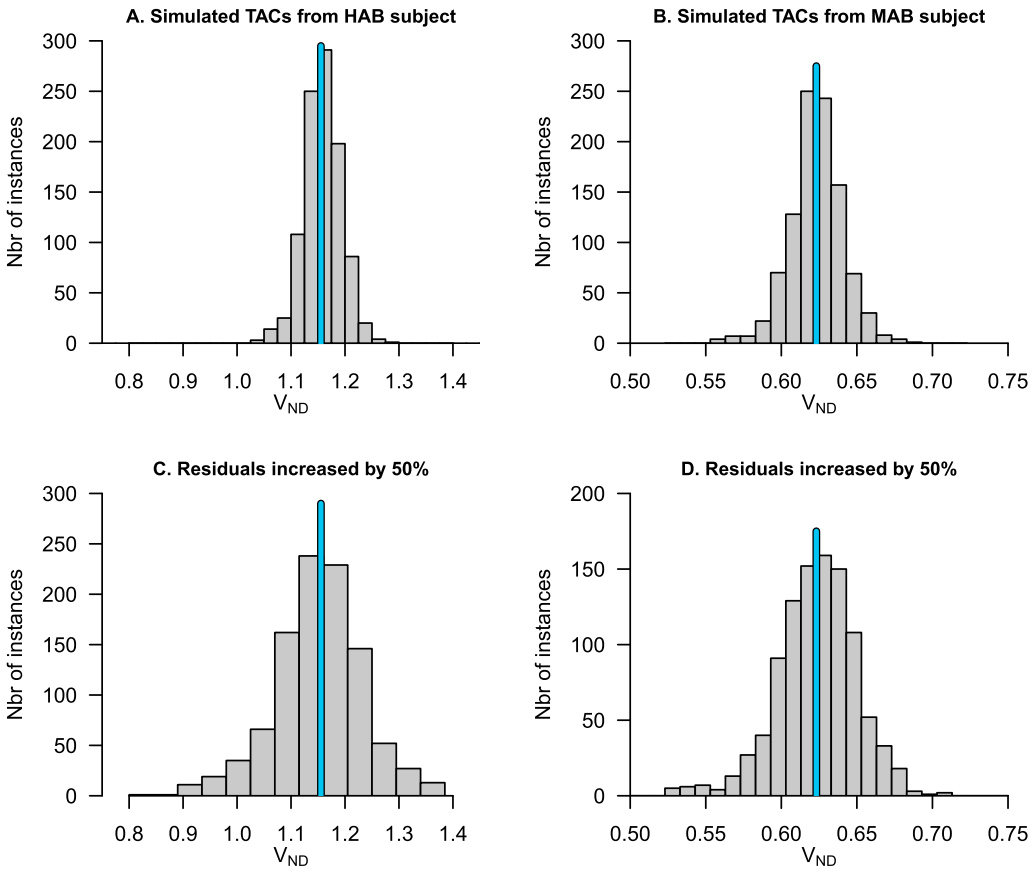

Fig. 1. Estimation of V_{ND} from simulated time-activity curves using SIME. In each plot, 1000 noise instances have been created and added onto a set of noise-free model curves obtained from a HAB subject (A and C) or a MAB subject (B and D) randomly selected from the KI [^{11}C]PBR28 database. In C and D the noise have been amplified by a factor of 1.5. The blue vertical lines indicate the "true" value of V_{ND}.

(i.e. V_S and BP_{ND}) was then assessed by calculating Hedges' g effect sizes of group differences, as well as percentage differences.

2.6. Test-retest analysis

For the subjects in the test-retest study (Collste et al., 2016), V_T values from GM and SIME-derived outcomes (V_{ND}, V_S and BP_{ND}) were obtained as described above for both test and retest PET examinations. The intraclass correlation coefficient (ICC) was used as a measure of test-retest reliability; percentage average absolute variability or test-retest variability (AbsVar) was used as a measure of reproducibility; and the standard error of measurement (SEM; (Weir, 2005)) was used as a measure of precision. AbsVar was included for reference since it is the most common metric reported in PET test-retest studies. However, caution is warranted when using AbsVar to compare outcome measures that are derived from each other by subtraction or addition (such as V_T and V_S), since these operations mathematically affects relative variability.

All kinetic modelling in this study was performed in Matlab 2014 (Mathworks, Natick, MA) and all statistical analyses were performed in R (v3.3.2, "Sincere Pumpkin Patch").

3. Results

3.1. Simulations

Fig. 1 shows the results from the simulation experiment. SIME was accurate in estimating the "true" V_{ND} value, for both genotypes (Panel A $V_{ND:True} = 1.15$, mean $V_{ND:SIME} = 1.17 \pm 0.035$SD, CoV = 3.0%, bias = +1.7%; Panel B $V_{ND:True} = 0.62$, mean $V_{ND:SIME} = 0.63 \pm 0.018$SD, CoV = 2.9%, bias = +1.6%). When amplifying the noise by 50%, SIME still provided accurate estimates of the "true" V_{ND}, although with lower precision (i.e. higher CoV) (Panel C $V_{ND:True} = 1.15$, mean $V_{ND:SIME} = 1.17 \pm 0.082$SD, CoV = 7.0%, bias = +1.7%; Panel D $V_{ND:True} = 0.62$, mean $V_{ND:SIME} = 0.63 \pm 0.027$SD, CoV = 4.3%, bias = +1.7%). We also

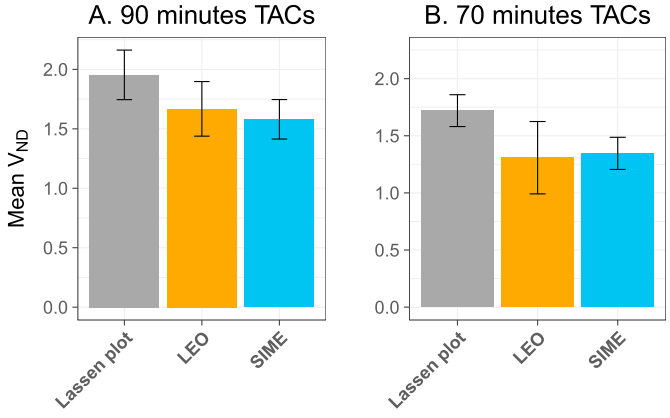

Fig. 2. Comparison of V_{ND} estimated using different methods. V_{ND} estimates from 5 HAB subjects undergoing a XBD173 blocking challenge, using the Lassen plot, Likelihood Estimation of Occupancy (LEO), and SIME (performed only on the baseline scans). On average, V_{ND} estimated with SIME was lower than that obtained using Lassen plot (90min: -19%, 70min: -22%), but similar to that obtained with LEO (90min: -3%, 70min: +6%). All three methods showed lower V_{ND} when shorter time activity curves (TACs) were used (Lassen plot: -12%; LEO: -22%; SIME -15%).

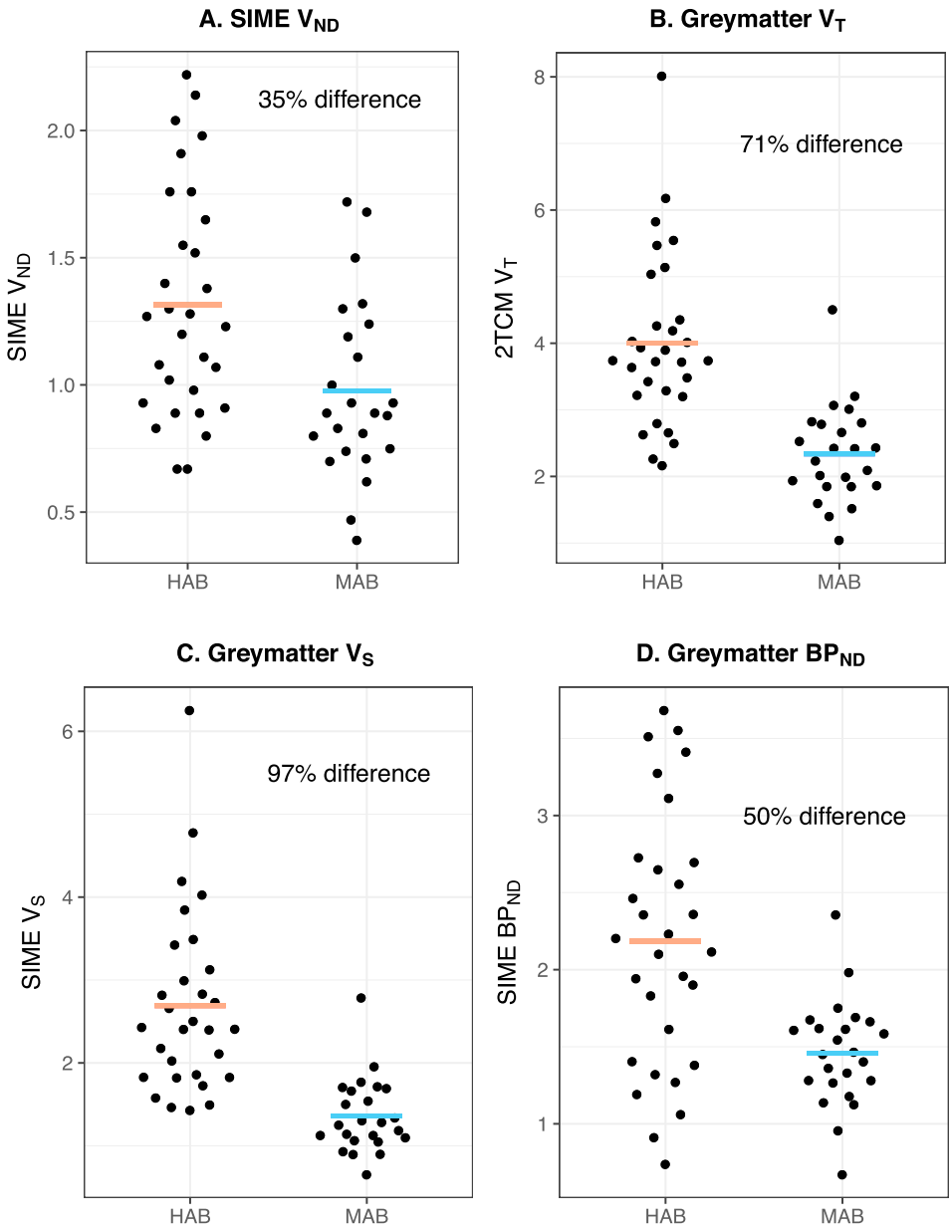

Fig. 3. Separation of genotype groups using different outcomes. There was a clear difference in SIME-V_{ND} between HABs and MABs (A). Mean percentage differences suggest that both V_T from 2TCM (B) and SIME-V_S (C) showed a strong separation between genotype groups, with HABs having double the V_S compared to MABs. SIME-BP_{ND} showed lower mean percentage separation between HABs and MABs (D) compared to V_T and V_S.

extracted average K_1/k_2 ratios from the unconstrained 2TCM performed on the simulated data. Mean K_1/k_2 showed both bias and low precision in estimating the underlying "true" V_{ND} value ($V_{ND:True} = 1.15$, mean $K_1/k_2 = 1.29 \pm 0.070$SD, CoV = 6%, bias = 12.2%, see Appendix A: Supplementary Information).

3.2. XBD173 competition

Fig. 2a shows the estimated V_{ND} values from the XBD173 competition data, with 90 min TACs, using the Lassen plot (mean $V_{ND} = 1.95 \pm 0.47$SD), LEO (mean $V_{ND} = 1.67 \pm 0.51$SD) and SIME (mean $V_{ND} = 1.58 \pm 0.37$SD) methods. Fig. 2b shows the estimated V_{ND} from 70 min TACs, using the Lassen plot (mean $V_{ND} = 1.72 \pm 0.31$SD), LEO (mean $V_{ND} = 1.31 \pm 0.71$SD) and SIME (mean $V_{ND} = 1.35 \pm 0.31$SD) methods. On average, SIME yielded lower V_{ND} values compared to the Lassen plot (90 min: -19%; 70 min: -22%) but displayed close correspondence to LEO (90 min: -3%; 70 min: +6%). For all three methods, estimated V_{ND} values were lower when shorter TACs were used (Lassen plot: mean −12%; LEO: mean −22%; SIME mean −15%). K_1/k_2 from the unconstrained 2TCM showed lower correspondence to both the Lassen-plot and LEO V_{ND} (Lassen-plot -41%; LEO -30%, see AFig 2 in Appendix A: Supplementary Information). For individual V_{ND} values of Lassen-plot, LEO and SIME, see AFig 3 in Appendix A: Supplementary Information.

3.3. Differences between HABs and MABs

Fig. 3A shows that there was a difference in SIME-V_{ND} between genotype groups, with HAB subjects showing on average 35% higher V_{ND} (mean = 1.31 ± 0.45SD) compared to MAB subjects (mean = 0.98 ± 0.35SD; $t = 3.13$, $df = 52$, $p = 0.0028$; Hedges' $g = 0.82$, 95% CI [0.26, 1.38]).

Fig. 3B–D shows how different outcome measures can differentiate between HAB and MAB subjects, using the GM ROI as target. V_T from the unconstrained 2TCM (HABs mean = 4.0 ± 1.29SD; MABs mean = 2.34 ±

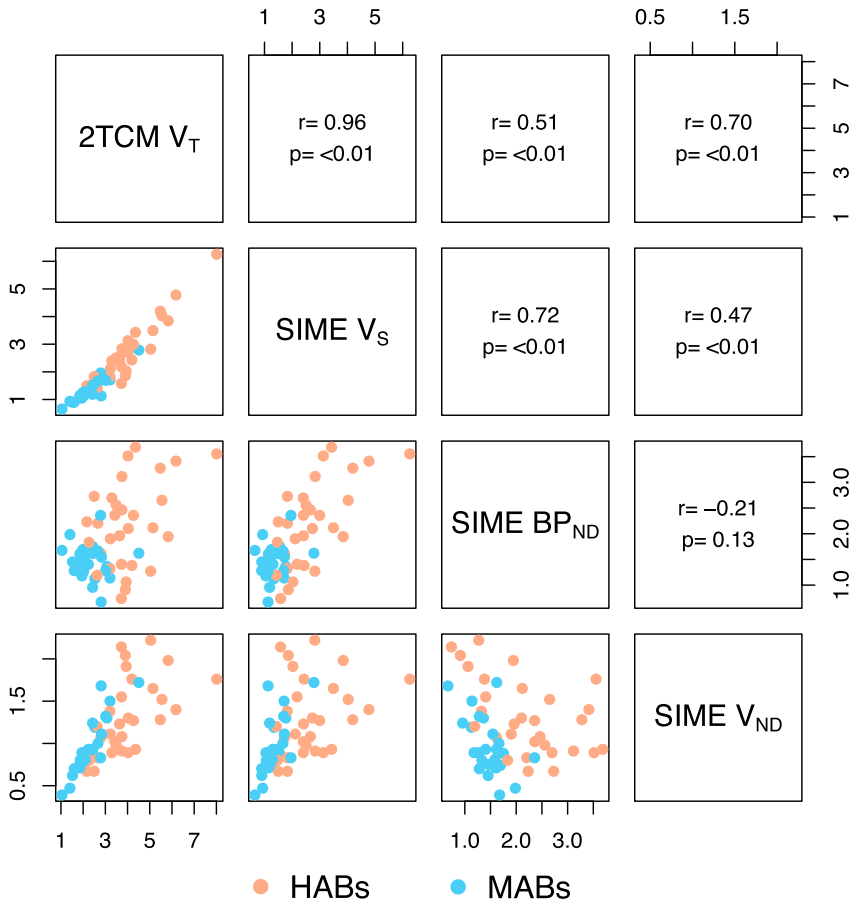

Fig. 4. Relationships between outcome measures. Scatter plots and Pearson's correlation coefficients (r) between V_T from 2TCM and V_S, BP_{ND} and V_{ND} from SIME with the whole grey matter as region of interest.

Table 2
Test-retest reliability, reproducibility and precision estimated for different outcome measures using the ICC, AbsVar and SEM. The whole of grey-matter was used as region of interest for V_T, V_S and BP_{ND}. PET1 is the first examination and PET2 is the follow-up examination.

Measure	Mean PET1	SD PET1	Mean PET2	SD PET2	ICC	AbsVar %	SEM
2TCM-V_T	3.41	1.86	3.65	1.84	0.94	17	0.43
SIME-V_{ND}	1.29	0.47	1.35	0.47	0.86	18	0.18
SIME-V_S	2.12	1.55	2.29	1.47	0.93	24	0.39
SIME-BP_{ND}	1.61	0.76	1.63	0.6	0.65	24	0.39

0.73SD; t = 6.0, df = 47, p = $2.6*10^{-7}$; Hedges' g = 1.53, 95% CI [0.92, 2.14]) and V_S from SIME (HABs mean = 2.69 ± 1.10SD; MABs mean = 1.36 ± 0.45SD; t = 6.0, df = 40, p = $4.3*10^{-7}$; Hedges' g = 1.50, 95% CI [0.89, 2.11]) showed similar separation between genotype groups, while BP_{ND} from SIME (HABs mean = 2.18 ± 0.83SD; MABs mean = 1.46 ± 0.34SD; t = 4.35, df = 40, p = $8.9*10^{-5}$; Hedges' g = 1.08, 95% CI [0.51, 1.66]) showed less separation.

3.4. Test-retest

Table 2 displays the test-retest metrics for all outcome measures, using the GM as target ROI. V_S from SIME showed excellent reliability (ICC > 0.9), while BP_{ND} showed poor reliability (ICC < 0.75) (Portney and Watkins, 2015).

3.5. Relationships between outcome measures

Fig. 5 shows the relationship between all different outcome measures and V_{ND} values from SIME. SIME-derived V_S values were highly correlated with both BP_{ND} from SIME (r = 0.72, t = 7.50, df = 52, p = $7.8*10^{-10}$) and V_T from the unconstrained 2TCM (r = 0.96, t = 24.31, df = 52, p = $4.6*10^{-30}$). V_{ND} from SIME showed a strong correlation to V_T (r = 0.70, t = 7.16, df = 52, p = $2.7*10^{-9}$), a moderate correlation to V_S (r = 0.47, t = 3.88, df = 52, p = 0.00029) and no correlation to BP_{ND} (r = −0.21, t = −1.55, df = 52, p = 0.13).

4. Discussion

Accurate, reliable and precise quantification of [^{11}C]PBR28 binding is of high interest for clinical research, as it would theoretically lead to easier detection of effects, allowing for higher power or lower sample sizes to be used, and thereby reducing the costs in PET TSPO studies. The purpose of this study was to evaluate a new method (SIME) for deriving estimates that reflect [^{11}C]PBR28 specific binding (Ogden et al., 2015), which has shown promising potential for [^{11}C]PBR28 group comparisons (Schain et al., 2018b).

We simulated [^{11}C]PBR28 TACs and examined the ability of SIME to estimate a known underlying V_{ND} value. The results showed that, in simulations, SIME-derived V_{ND} values were both accurate and precise (Fig. 1A and B). This was also the case when the amount of noise in the TACs was increased above realistic levels, suggesting that SIME is robust to high levels of noise (Fig. 1C and D).

We also compared SIME against "gold standard" measures of V_{ND} by using data from a XBD173 blocking challenge (Owen et al., 2014). SIME, applied to the baseline scans, yielded V_{ND} values in the same range as the

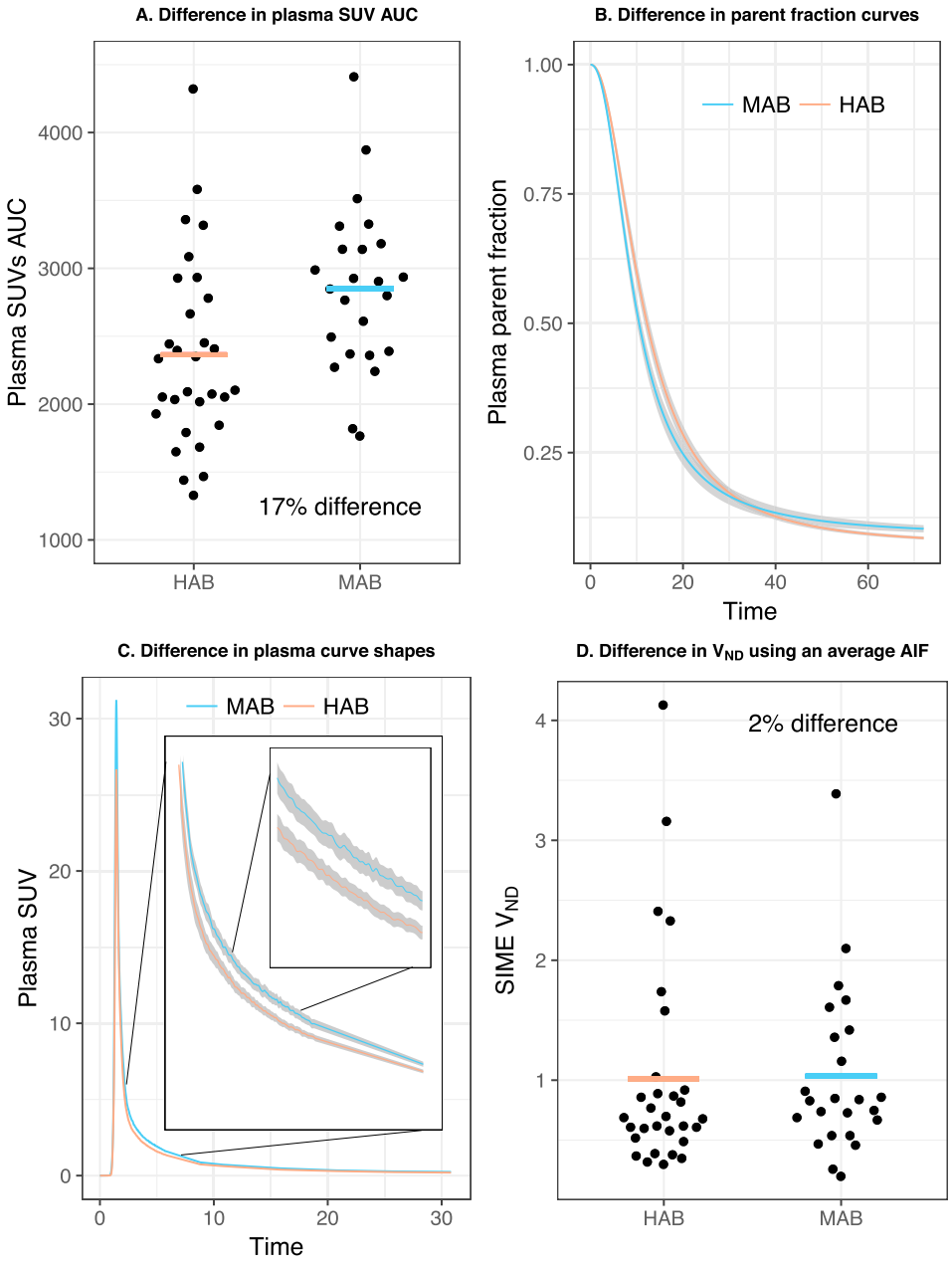

Fig. 5. Differences in AIF between HABs and MABs. There was difference in the magnitude and shape of AIF SUV between genotype groups (A), with HABs showing 17% lower AUC (mean = 2365 ± 690SD) compared to MABs (mean = 2851 ± 608SD; t = −2.75, df = 52, p = 0.0083; Hedges' g = −0.73, 95%CI [-1.28, −0.18]), and a steeper post-peak decay of radioactivity in plasma (C). When using the same normalized AIF for all subjects (D), V_{ND} was similar between groups (HABs: mean = 1.01 ± 0.90SD; MABs mean = 1.03 0.7; t = −0.11, df = 52, p = 0.91; Hedges' g = −0.029, 95%CI [-0.57, 0.51]. The shaded area around the lines (B and C) represent 1SE. The average parent fraction curve (B) showed significant differences between HABs and MABs at 10 min and 70 min. There was no overlap between the two average AIF curves in the interval seen in the enhanced subplot (C), as determined by 95% confidence intervals.

recently developed LEO technique (Schain et al., 2018a), but lower than V_{ND} values obtained with the revised Lassen plot (Fig. 2). Both the Lassen plot and LEO showed lower V_{ND} when shorter TACs were analyzed, suggesting that estimates of V_{ND} are sensitive to scan duration. This trend was also reflected by the SIME method, which showed similar percentage decrease in V_{ND}.

In addition to the above, we evaluated how SIME-V_{ND} compared to V_{ND} derived using K_1 and k_2 from the unconstrained 2TCM. K_1/k_2 showed higher bias and lower precision in the simulations, and less correspondence to Lassen-plot and LEO, compared to the SIME-V_{ND} (see Appendix A: Supplementary Information). This suggest that SIME show higher accuracy compared to V_{ND} estimated directly from the unconstrained 2TCM.

In the 2TCM, V_{ND} only reflects non-specific binding and free radioligand in tissue, which together constitute the non-displaceable binding. Since it is generally believed that the genotype only affects the radioligand's affinity to TSPO, it follows that no difference in V_{ND} estimates between genotype groups is expected. However, in this study SIME-derived V_{ND} estimates showed a clear difference between HAB and MAB subjects (Fig. 3A).

We suggest three potential hypotheses to explain this observation: 1) the SIME approach is sensitive to "spill in" from the specific compartment to the non-displaceable compartment, so that SIME-derived V_{ND} values are inflated by high V_S values; 2) there is a systematic difference in the measurement of the AIF for HABs and/or MABs that affects the estimated V_{ND}; 3) a subject's V_{ND} is dependent on the TSPO genotype (such as an TSPO affinity-dependent transport across the blood-brain barrier).

To assess the first hypothesis, we performed additional simulations (see Appendix A: Supplementary Information) in which the k_3/k_4 ratio (i.e., the BP_{ND}) was both substantially increased and decreased, respectively, while the true V_{ND} was kept constant. These simulations showed that SIME produced similar estimates of V_{ND} regardless of the k_3/k_4 values (Figure A4), suggesting that hypothesis 1 above is an unlikely explanation to the observed difference in V_{ND} between genotype groups.

As for the second hypothesis, we calculated the area under the curve (AUC) of each subject's AIF (expressed as standard uptake values, SUV),

and extracted fitted parent fraction curves (see Appendix A: Supplementary Information for a description of the methods). We observed a clear difference between genotype groups in both AUC and shape of the plasma TACs, as well as differences in the parent fraction curves (Fig. 5B–D). When modelling the subjects with SIME using an average AIF for both genotypes, the differences in SIME-V_{ND} between HABs and MABs disappeared (Fig. 5), an observation consistent with hypothesis 2), but also with 3) above.

We also tested if the whole greymatter K_1 values, extracted from the unconstrained 2TCM, differed between genotype groups. There was a small significant difference between HABs and MABs ($t = 2.02$, $df = 46$, $p = 0.049$), with HABs showing on average higher K_1 values. Although the effect size was small (Hedge's $g = 0.5$) this provides some support for hypothesis 3) above. However, conclusions about underlying biology should not be drawn solely based on the performance of models. To date, there exists no published [^{11}C]PBR28 blocking data examining V_{ND} in MAB subjects. Hence, the observed difference between genotypes cannot be fully verified, and this phenomenon warrants further investigation.

In this study, we compared SIME-derived binding values between TSPO genotype groups (Fig. 3). When using individual AIFs, SIME V_S in HABs (mean = 2.69) was almost exactly double the value of V_S in MAB subjects (mean = 1.36). Assuming SIME-V_S is valid, this is to be expected since the low-affinity-binder allele shows negligible binding of [^{11}C]PBR28 to TSPO, so that HAB subjects effectively have twice as many TSPO binding sites as MAB subjects (Owen et al., 2012).

The reliability of [^{11}C]PBR28 V_S and BP_{ND} in GM was evaluated using a test-retest data set. SIME-derived V_S showed high reliability and precision, reaching the threshold recommended for clinical use (ICC > 0.9) (Portney and Watkins, 2015). SIME-derived BP_{ND} showed both less separation between genotype groups (Fig. 3D) and lower reliability (Table 2), compared to both V_T and SIME-derived V_S. One potential explanation for these findings is that small amounts of measurement error in both the numerator (V_S) and the denominator (V_{ND}) of SIME-derived BP_{ND} (eq 2) leads to an amplified error in the quotient, while this is not the case for subtraction carried out to calculate V_S (eq 1).

The results of this study supports the use of SIME-derived V_S as an outcome measure for future [^{11}C]PBR28 examinations in complement to e.g. V_T from the unconstrained 2TCM. This is in line with the principle that V_S reflects more directly the level of specific binding than V_T, and a difference of interest between subjects or groups is expected to be confined to only V_S. For instance, if V_{ND} represents 30% of the signal, a 25% increase in V_S would be reflected by a 17.5% increase in V_T, assuming both outcomes show equal variance. These hypothesized differences in sensitivity should be further tested in clinical studies using [^{11}C]PBR28. To facilitate this, we publicly share all code for executing SIME in Matlab (github.com/martinschain/SIME). SIME is also implemented in the open-source R-package *kinfitr* for kinetic modelling of brain PET data (github.com/mathesong/kinfitr).

Conflicts of interest

The authors declare no conflict of interest.

Author contribution

PPS conceived of the study. PPS, MS, FZ, TO and SC designed the study. TO, FZ and SC supervised the study. SC, RG and IR contributed to the acquisition of data. MS and PPS performed the image analysis and modelling. PPS, MS and SC drafted the manuscript. All authors revised the manuscript and approved the final version for publication.

Acknowledgements

We thank David Owen, Katarina Varnäs, Anton Forsberg and Zsolt Cselényi for their help during the course of this investigation. We also thank the members of the Karolinska Institutet PET group, Invicro LLC, and the Division of Molecular Imaging and Neuropathology at the New York State Psychiatric Institute for their assistance during the study.

M.S was supported by a NARSAD Young Investigator Grant from the Brain and Behavior Research Foundation. S.C. was supported by the Swedish Research Council (Grant No. 523-2014-3467).

Appendix A. Supplementary data

Supplementary data to this article can be found online at https://doi.org/10.1016/j.neuroimage.2018.11.020.

References

Bloomfield, P.S., Selvaraj, S., Veronese, M., Rizzo, G., Bertoldo, A., Owen, D.R., Bloomfield, M.A.P., Bonoldi, I., Kalk, N., Turkheimer, F., 2015. Microglial activity in people at ultra high risk of psychosis and in schizophrenia: an [11C] PBR28 PET brain imaging study. Am. J. Psychiatry 173, 44–52.

Briard, E., Zoghbi, S.S., Imaizumi, M., Gourley, J.P., Shetty, H.U., Hong, J., Cropley, V., Fujita, M., Innis, R.B., Pike, V.W., 2007. Synthesis and evaluation in monkey of two sensitive 11C-labeled aryloxyanilide ligands for imaging brain peripheral benzodiazepine receptors in vivo. J. Med. Chem. 51, 17–30.

Chauveau, F., Boutin, H., Van Camp, N., Dollé, F., Tavitian, B., 2008. Nuclear imaging of neuroinflammation: a comprehensive review of [11 C] PK11195 challengers. Eur. J. Nucl. Med. Mol. Imag. 35, 2304–2319.

Collste, K., Forsberg, A., Varrone, A., Amini, N., Aeinehband, S., Yakushev, I., Halldin, C., Farde, L., Cervenka, S., 2016. Test–retest reproducibility of [11C] PBR28 binding to TSPO in healthy control subjects. Eur. J. Nucl. Med. Mol. Imag. 43, 173–183.

Collste, K., Plavén-Sigray, P., Fatouros-Bergman, H., Victorsson, P., Schain, M., Forsberg, A., Amini, N., Aeinehband, S., Erhardt, S., Halldin, C., Flyckt, L., Farde, L., Cervenka, S., 2017. Lower levels of the glial cell marker TSPO in drug-naive first-episode psychosis patients as measured using PET and [11C]PBR28. Mol. Psychiatr. 22, 850–856. https://doi.org/10.1038/mp.2016.247.

Crawshaw, A.A., Robertson, N.P., 2017. The role of TSPO PET in assessing neuroinflammation. J. Neurol. 264, 1825–1827.

Cunningham, V.J., Rabiner, E.A., Slifstein, M., Laruelle, M., Gunn, R.N., 2010. Measuring drug occupancy in the absence of a reference region: the Lassen plot re-visited. J. Cereb. Blood Flow Metab. 30, 46–50. https://doi.org/10.1038/jcbfm.2009.190.

Fregonara, P.Z., Richards, E., Newman, L., Fujita, M., Niciu, M., Machado-Vieira, R., Salvadore, G., Kolb, H., Drevets, W., Zoghbi, S., 2017. Unmedicated major depressive disorder is associated with neuroinflammation. J. Nucl. Med. 58, 139.

Fujita, M., Kobayashi, M., Ikawa, M., Gunn, R.N., Rabiner, E.A., Owen, D.R., Zoghbi, S.S., Haskali, M.B., Telu, S., Pike, V.W., Innis, R.B., 2017. Comparison of four 11C-labeled PET ligands to quantify translocator protein 18 kDa (TSPO) in human brain: (R)-PK11195, PBR28, DPA-713, and ER176—based on recent publications that measured specific-to-non-displaceable ratios. EJNMMI Res. 7. https://doi.org/10.1186/s13550-017-0334-8.

Heneka, M.T., Carson, M.J., El Khoury, J., Landreth, G.E., Brosseron, F., Feinstein, D.L., Jacobs, A.H., Wyss-Coray, T., Vitorica, J., Ransohoff, R.M., 2015. Neuroinflammation in Alzheimer's disease. Lancet Neurol. 14, 388–405.

Ichise, M., Toyama, H., Innis, R.B., Carson, R.E., 2002. Strategies to improve neuroreceptor parameter estimation by linear regression analysis. J. Cerebr. Blood Flow Metabol. 22, 1271–1281.

Innis, R.B., Cunningham, V.J., Delforge, J., Fujita, M., Gjedde, A., Gunn, R.N., Holden, J., Houle, S., Huang, S.C., Ichise, M., Iida, H., Ito, H., Kimura, Y., Koeppe, R.A., Knudsen, G.M., Knuuti, J., Lammertsma, A.A., Laruelle, M., Logan, J., Maguire, R.P., Mintun, M.A., Morris, E.D., Parsey, R., Price, J.C., Slifstein, M., Sossi, V., Suhara, T., Votaw, J.R., Wong, D.F., Carson, R.E., 2007. Consensus nomenclature for in vivo imaging of reversibly binding radioligands. J. Cerebr. Blood Flow Metabol. 27, 1533–1539. https://doi.org/10.1038/sj.jcbfm.9600493.

Jučaite, A., Cselényi, Z., Arvidsson, A., Åhlberg, G., Julin, P., Varnäs, K., Stenkrona, P., Andersson, J., Halldin, C., Farde, L., 2012. Kinetic analysis and test-retest variability of the radioligand [11C](R)-PK11195 binding to TSPO in the human brain - a PET study in control subjects. EJNMMI Res. 2.

Kanegawa, N., Collste, K., Forsberg, A., Schain, M., Arakawa, R., Jucaite, A., Lekander, M., Höglund, C.O., Kosek, E., Lampa, J., 2016. In vivo evidence of a functional association between immune cells in blood and brain in healthy human subjects. Brain. Behav. Immun. 54, 149–157.

Kobayashi, M., Jiang, T., Telu, S., Zoghbi, S.S., Gunn, R.N., Rabiner, E.A., Owen, D.R., Guo, Q., Pike, V.W., Innis, R.B., 2017. 11C-DPA-713 has much greater specific binding to translocator protein 18 kDa (TSPO) in human brain than 11C-(R)-PK11195. J. Cerebr. Blood Flow Metabol. 38 , 393–403.

Kreisl, W.C., Fujita, M., Fujimura, Y., Kimura, N., Jenko, K.J., Kannan, P., Hong, J., Morse, C.L., Zoghbi, S.S., Gladding, R.L., Jacobson, S., Oh, U., Pike, V.W., Innis, R.B., 2010. Comparison of [(11)C]-(R)-PK 11195 and [(11)C]PBR28, two radioligands for translocator protein (18 kDa) in human and monkey: implications for positron emission tomographic imaging of this inflammation biomarker. Neuroimage 49, 2924–2932. https://doi.org/10.1016/j.neuroimage.2009.11.056.

Kreisl, W.C., Lyoo, C.H., Liow, J.-S., Wei, M., Snow, J., Page, E., Jenko, K.J., Morse, C.L., Zoghbi, S.S., Pike, V.W., 2016. 11 C-PBR28 binding to translocator protein increases with progression of Alzheimer's disease. Neurobiol. Aging 44, 53–61.

Lagarde, J., Sarazin, M., Bottlaender, M., 2017. In vivo PET imaging of neuroinflammation in Alzheimer's disease. J. Neural. Transm. 847–867.
Liu, G., Middleton, R.J., Hatty, C.R., Kam, W.W., Chan, R., Pham, T., Harrison-Brown, M., Dodson, E., Veale, K., Banati, R.B., 2014. The 18 kDa translocator protein, microglia and neuroinflammation. Brain Pathol. 24, 631–653.
Logan, J., Fowler, J.S., Volkow, N.D., Wang, G.-J., Ding, Y.-S., Alexoff, D.L., 1996. Distribution volume ratios without blood sampling from graphical analysis of PET data. J. Cerebr. Blood Flow Metabol. 16, 834–840.
Lyoo, C.H., Ikawa, M., Liow, J.-S., Zoghbi, S.S., Morse, C.L., Pike, V.W., Fujita, M., Innis, R.B., Kreisl, W.C., 2015. Cerebellum can serve as a pseudo-reference region in Alzheimer disease to detect neuroinflammation measured with PET radioligand binding to translocator protein. J. Nucl. Med. 56, 701–706.
Matheson, G.J., Plavén-Sigray, P., Forsberg, A., Varrone, A., Farde, L., Cervenka, S., 2017. Assessment of simplified ratio-based approaches for quantification of PET [^{11}C] PBR28 data. EJNMMI Res. 7. https://doi.org/10.1186/s13550-017-0304-1.
Naganawa, M., Gallezot, J.-D., Rossano, S., Carson, R.E., 2017. Quantitative PET imaging in drug development: estimation of target occupancy. In: Bulletin of Mathematical Biology. Springer, pp. 1–34. https://doi.org/https://doi.org/10.1007/s11538-017-0374-2.
Nair, A., Veronese, M., Xu, X., Curtis, C., Turkheimer, F., Howard, R., Reeves, S., 2016. Test-retest analysis of a non-invasive method of quantifying [11C]-PBR28 binding in Alzheimer's disease. EJNMMI Res. 6.
Ogden, R.T., Zanderigo, F., Parsey, R.V., 2015. Estimation of in vivo nonspecific binding in positron emission tomography studies without requiring a reference region. Neuroimage 108, 234–242.
Owen, D.R., Guo, Q., Kalk, N.J., Colasanti, A., Kalogiannopoulou, D., Dimber, R., Lewis, Y.L., Libri, V., Barletta, J., Ramada-Magalhaes, J., 2014. Determination of [11C]PBR28 binding potential in vivo: a first human TSPO blocking study. J. Cerebr. Blood Flow Metabol. 34, 989–994.
Owen, D.R., Yeo, A.J., Gunn, R.N., Song, K., Wadsworth, G., Lewis, A., Rhodes, C., Pulford, D.J., Bennacef, I., Parker, C.A., StJean, P.L., Cardon, L.R., Mooser, V.E., Matthews, P.M., Rabiner, E.A., Rubio, J.P., 2012. An 18-kDa translocator protein (TSPO) polymorphism explains differences in binding affinity of the PET radioligand PBR28. J. Cerebr. Blood Flow Metabol. 32, 1–5. https://doi.org/10.1038/jcbfm.2011.147.
Park, E., Gallezot, J.-D., Delgadillo, A., Liu, S., Planeta, B., Lin, S.-F., O'Connor, K.C., Lim, K., Lee, J.-Y., Chastre, A., 2015. 11C-PBR28 imaging in multiple sclerosis patients and healthy controls: test-retest reproducibility and focal visualization of active white matter areas. Eur. J. Nucl. Med. Mol. Imag. 42, 1081–1092.
Plavén-Sigray, P., Matheson, G.J., Cselényi, Z., Jučaite, A., Farde, L., Cervenka, S., 2018. Test-retest reliability and convergent validity of (R)-[11C] PK11195 outcome measures without arterial input function. EJNMMI Res. 8 bioRxiv 298992.
Portney, L.G., Watkins, M.P., 2015. Foundations of Clinical Research: Applications to Practice, third ed. FA Davis, Philadelphia.
Rizzo, G., Veronese, M., Tonietto, M., Zanotti-Fregonara, P., Turkheimer, F.E., Bertoldo, A., 2014. Kinetic modeling without accounting for the vascular component impairs the quantification of [11C] PBR28 brain PET data. J. Cerebr. Blood Flow Metabol. 34, 1060–1069.
Schain, M., Zanderigo, F., Ogden, R.T., 2018a. Likelihood estimation of drug occupancy for brain PET studies. Neuroimage 178, 255–265.
Schain, M., Zanderigo, F., Ogden, R.T., Kreisl, W.C., 2018b. Non-invasive estimation of [11 C] PBR28 binding potential. Neuroimage 169, 278–285.
Slifstein, M., Laruelle, M., 2001. Models and methods for derivation of in vivo neuroreceptor parameters with PET and SPECT reversible radiotracers. Nucl. Med. Biol. 28, 595–608.
Tamm, S., Cervenka, S., Forsberg, A., Estelius, J., Grunewald, J., Gyllfors, P., Karshikoff, B., Kosek, E., Lampa, J., Lensmar, C., 2017. Evidence of fatigue, disordered sleep and peripheral inflammation, but not increased brain TSPO expression, in seasonal allergy: a [11C] PBR28 PET study. Brain Behav. Immun. 68, 146–157.
van der Doef, T.F., Doorduin, J., van Berckel, B.N.M., Cervenka, S., 2015. Assessing brain immune activation in psychiatric disorders: clinical and preclinical PET imaging studies of the 18-kDa translocator protein. Clin. Transl. Imaging 3, 449–460.
Varnäs, K., Varrone, A., Farde, L., 2013. Modeling of PET data in CNS drug discovery and development. J. Pharmacokinet. Pharmacodyn. 40, 267–279.
Venneti, S., Lopresti, B.J., Wiley, C.A., 2013. Molecular imaging of microglia/macrophages in the brain. Glia 61, 10–23.
Venneti, S., Lopresti, B.J., Wiley, C.A., 2006. The peripheral benzodiazepine receptor (Translocator protein 18kDa) in microglia: from pathology to imaging. Prog. Neurobiol. 80, 308–322.
Veronese, M., Marques, T., Bloomfield, P.S., Rizzo, G., Singh, N., Jones, D., Agushi, E., Mosses, D., Bertoldo, A., Howes, O., Roncaroli, F., Turkheimer, F.E., 2017. Kinetic modelling of [11C]PBR28 for 18kDa Translocator Protein PET data: a validation study of vascular modelling in the brain using XBD173 and tissue analysis. J. Cerebr. Blood Flow Metabol. 38, 1227–1242.
Wee Yong, V., 2010. Inflammation in neurological disorders: a help or a hindrance? Neuroscience 16, 408–420.
Weir, J.P., 2005. Quantifying test-retest reliability using the intraclass correlation coefficient and the SEM. J. Strength Condit Res. 19, 231–240.